IEEE Access
Multidisciplinary ⋮ Rapid Review ⋮ Open Access Journal

Received 2 August 2024, accepted 20 August 2024, date of publication 26 August 2024, date of current version 5 September 2024.

Digital Object Identifier 10.1109/ACCESS.2024.3449291

RESEARCH ARTICLE

Comprehensive Analytical Model for Exploring the Dominant Scattering Mechanism of Two-Dimensional MoS_2 FETs

FATIMAH AROFIATI NOOR[1], (Member, IEEE), IBNU SYUHADA[2], TOTO WINATA[1], AND KHAIRURRIJAL KHAIRURRIJAL[1], (Member, IEEE)

[1]Physics and Technology of Advanced Materials, Department of Physics, Faculty of Mathematics and Natural Sciences, Institut Teknologi Bandung, Bandung 40132, Indonesia
[2]Yayasan Cahaya Putra Ilmu, Cilegon, Banten 42411, Indonesia

Corresponding author: Fatimah Arofiati Noor (fatimah@itb.ac.id)

This work was supported by the Institut Teknologi Bandung (ITB) through the "Riset Unggulan ITB" research grant 2022.

ABSTRACT This work proposes a comprehensive analytical model for two-dimensional molybdenum disulfide (MoS_2) field-effect transistors (FETs). This model incorporates single-particle and transport relaxation times intended to investigate the dominant scattering mechanism in these devices. Our results show that in MoS_2 FETs with a short channel length, there is a shift in short-range scattering from anisotropy mediated by the tunneling mechanism toward isotropy due to thermionic emission when the gate voltage is increased, which is in line with density functional theory (DFT). Meanwhile, long-range scattering by the interface traps electrons responsible for carrier transport in long-channel MoS_2 FETs. We validate the model against experimental data on I_d-V_d and I_d-V_g characteristics, including mobility. The validations indicate that our model can accurately capture negative differential resistance (NDR) phenomenon and interface traps in MoS_2 FETs. Therefore, our model is suitable to gain detailed insight into the dominant scattering mechanism directly from the current-voltage characteristics curve, minimizing the need for complex measurements and simulations.

INDEX TERMS Dominant scattering mechanism, MoS_2 FETs, negative drain resistance, interface traps, quantum relaxation time, transport relaxation time.

I. INTRODUCTION

Understanding MoS_2 transistor drain current performance at the nanoscale remains one of the most challenging aspects of experimental work in this field. Therefore, using theoretical studies to uncover the scattering mechanisms influencing performance can support device development. Das Sarma and colleagues have conducted several studies to distinguish the characteristic single-particle and transport relaxation times, denoted τ_q and τ_t, respectively [1], [2]. The single-particle relaxation time or quantum lifetime, which determines the quantum level broadening $\Gamma \equiv \hbar/2\tau_q$, is a measure of the time for which electrons remain in momentum eigenstates before scattering. Meanwhile, the transport relaxation time is related to conductivity, $\sigma \propto \tau_t$. Observing characteristic times is valuable for identifying or analyzing the dominant scattering.

Theoretical simulations have been conducted for quantum-based scattering dominance, such as using Green's function to examine magnon existence influence [3], [4] and applying the first-principle method for electron-phonon interactions in two-dimensional materials [5], [6]. These methods have commonly applied the Boltzmann transport equation (BTE) to determine characteristic times, which can drive complex calculations, especially first-principle simulations of a few femtoseconds. Alternatively, several recent numerical approaches have studied this characteristic to understand the Anderson localization effect in doped

The associate editor coordinating the review of this manuscript and approving it for publication was Ye Zhou.

semiconductors [7], the failure of the Wiedemann-Franz law in graphene [8], and Weyl nodes due to residual disorder in WTe_2 [9]. Regarding monolayer MoS_2, a theoretical model has been developed for the operational characteristic of a transition-metal dichalcogenide thin-film transistor by considering trapped charges near the channel interface [10]. This model applies relaxation time approximation and the Fourier-transformed Coulomb potential due to the charge to describe the Coulomb scattering mechanism in solving the BTE. Compared with other methods, this model does not require complex quantum calculations and is consistent with experimental data. Nevertheless, this study explains the transistor I-V characteristic model using a traditional quadratic equation for the applied. However, the quadratic equation cannot capture the negative differential resistance (NDR) phenomenon commonly encountered in two-dimensional MoS_2 materials [11], [12], [13]. The study that combined Green's function and the first-principle method shows that the NDR phenomenon on two-dimensional materials makes that the ballistic limit model cannot be used for this material [14].

Numerous efforts have been made to improve the small transistor model by incorporating small amounts of scattering effects into a quasi-ballistic model to fit experimental data. The models commonly use a critical distance concept in the transmission function to account for scattering effects on the drain current performance of the device [15], [16], [17], [18]. Critical distance allows for the region consideration where a dominant scattering occurs in the transistor channel. Studies have developed models based on the Landauer-Buttiker formula assuming the Wentzel-Kramers-Brillouin (WKB) approximation to the transmission function [19], [20], [21], [22]. Due to different paradigms, the WKB approximation does not work well with small scattering mechanisms, especially scattering on carriers with energies above barrier potential. Small scattering works when the barrier potential is small enough compared with the energy of the particle [23], whereas WKB is valid if the potential is a smooth function of the coordinates [24]. These paradigms are also one of the reasons the ballistic series model requires further development to capture the NDR phenomenon in MoS_2 transistors.

Here, we present a comprehensive analytical transport model to describe the drain current performance of a two-dimensional MoS_2 nanoscale transistor with the NDR phenomenon and interface traps. Our model differs from other nanoscale transistor transport models that depend on critical distances. The model aims to identify the dominant scattering mechanism of the device by calculating the ratio between single-particle and transport relaxation times in the framework of the Landauer-Buttiker formula extension. Our approach to this extension is to modify the WKB approximation in the transmission formula to have the same order of magnitude as small scattering. In this manner, we can obtain a relationship between the relaxation time ratio and transmission. To support our work, we use data from a monolayer MoS_2 FET to measure the accuracy and compare it with statistical measures. Another advantage is that our model consistently captures the drain-induced barrier lowering (DIBL) phenomenon. Using our model analysis, we found that the scattering mechanism of a monolayer MoS_2 FET agrees with DFT and Monte Carlo simulation results. Therefore, our model is beneficial in gaining detailed insight into the scattering mechanism directly from the current-voltage characteristics curve, leading to cost savings for complex measurements and simulations.

II. THEORETICAL MODEL

To model a two-dimensional MoS_2 FET drain current with characteristic times embedded in transmission, we consider a general nanoscale metal-oxide-semiconductor field-effect transistor (MOSFET) in which carrier transport occurs along the channel length. A step-like potential profile confines carriers along the channel width. A sharp triangle-like potential confines carriers at the metal-oxide-semiconductor (MOS) interface and contains discrete band energy levels for electronic states along the depth. For a double-gate (DG) MOSFET, the interface layer construction modifies the band energy profile. We express the drain current model with the Landauer-Büttiker formula as follows [25], [26], [27], [28]:

$$I_d = \frac{q}{\pi\hbar} \sum_{v,n_y,n_z} \int \left(f_s(E) - f_d(E)\right) T(E) dE. \tag{1}$$

Here,

$$f_{(s/d)}(E) = \left(1 + \exp\left(\frac{E - E_{F(s/d)}}{k_B T_e}\right)\right)^{-1}$$

is the Fermi distribution function of the source (drain). $T_e 0$, k_B, $T(E)$, E_F, n_y, and n_z represent temperature, Boltzmann constant, transmission coefficient in the channel at energy E, Fermi energy, and quantum numbers for channel confinement in the width and depth directions, respectively. Our approach to resolving the paradigm is to express the carrier reflection as follows, such that the WKB approximation has the same order of magnitude as small scattering [29]:

$$R = \frac{r^2}{4} \left| \int_0^{k_0 L} U(\varepsilon\xi) e^{2i\xi} d\xi \right|^2, \tag{2}$$

where $r = \frac{E_{n_z}(x_{max})}{E - E_{n_y}}$, $\varepsilon = (k_0 L)^{-1}$, $\xi = k_0 x$, $k_0 = h^{-1}\sqrt{2m_x\left(E - E_{n_y}\right)}$, and $U(\varepsilon\xi) = \frac{E_{n_z}}{E_{n_z}(x_{max})}$. E_{n_z} represents the energy level associated with the n_z-th mode in the channel depth direction as a function of position along the channel length, x. Meanwhile, $E_{n_z}(x_{max})$ refers to the highest barrier at x_{max}. E_{n_y}, m_x, and L are energy levels associated with the n_y-th mode in channel width, conductivity effective mass, and channel length, respectively. The integral in Eq. (2) is challenging due to the dependency of the barrier profile on carrier distribution in the channel. For simplicity, we make two assumptions: the barrier profile decreases slowly to the drain and only considers scattering

around the barrier potential peak, so $r \sim 1$ and $E_{n_z} = E_{n_z}(x_{max})\,\delta(\varepsilon(\xi - \xi_{max}))$, where $\xi_{max} = k_0 x_{max}$. The formula for E_{n_z} used in this study is unsophisticated because it only accounts for the dominant scattering event at the peak of the barrier inside the nanotransistor channel. With these assumptions, the reflection is $R \approx \frac{2m_x L^2\left(E-E_{n_y}\right)}{4\hbar^2}$. According to $T = 1 - R$, the transmission has the following formula:

$$T = 1 - \frac{2m_x L^2\left(E - E_{n_y}\right)}{4\hbar^2}. \tag{3}$$

With Eq. (3), we extend the Landauer-Buttiker formula of Eq. (1) to include a small scattering mechanism. The model becomes:

$$I_d = \frac{q}{\pi\hbar}\sum_{v,n_y,n_z}\int (f_s(E) - f_d(E))\,dE - \frac{1}{4}\frac{q}{\pi\hbar}\frac{2m_x L^2}{\hbar^2}\sum_{v,n_y,n_z}\int (f_s(E) - f_d(E))\left(E - E_{n_y}\right)dE. \tag{4}$$

The first term in Eq. (4) represents the ballistic current, and the integration result is similar to the Natori model [28]. The second term is a correction due to small scattering when the carrier crosses the channel. Similar to the work of Natori, we replace the n_y summation by multiplying the integration over energy with the one-dimensional density of the state function and $\sum_{v,n_z}$ with M_v for the single sub-band approximation, which represents the carriers population fraction at the lowest level. Integrating Eq. (4) yields:

$$I_d = WI_0\left(F_{1/2}(u) - F_{1/2}(u - u_d)\right) - \zeta\frac{2m_x L^2}{\hbar}\frac{k_B T_e}{\hbar}\frac{2}{3}WI_0\left(F_{3/2}(u) - F_{3/2}(u - u_d)\right), \tag{5}$$

where parameters W is channel width, $u_d = \frac{qV_d}{k_B T_e}\Delta$, $I_0 = I_{0t}M_v$, $Q_{inv} = C_{ox}\left(V_g - V_{th} + \theta V_d\right)$, $\rho = \alpha\rho_0$, $\rho_0 = \frac{Q_{inv}}{Q_0 M_v}$, and

$$u = \ln\left[\sqrt{(1 + e^{u_d})^2 + 4e^{u_d}\left(e^{\rho} - 1\right)} - \left(1 + e^{u_d}\right)\right] - \ln 2.$$

Here, we add the dimensionless parameter, ζ, to Eq. (5) to anticipate the numerical approach to the final integration. This parameter has the physical meaning of a small scattering correction. When ζ is zero then the small scattering disappears. I_{0t} and Q_0 depend on the material properties of the transistor and the temperature. ρ_0 represents the average charge carrier density at the lowest level in a dimensionless unit. Furthermore, we use the strong inversion assumption on Q_{inv} to simplify the current study. Δ is a parameter that determines the physical properties of the body factor, m, using $\Delta = 1/m$. We note the Δ in this study as the body factor inverse. The θ parameter represents the DIBL to account for the short-channel effect (SCE). According to the experimental results, the oxide capacitance tends to increase for large MOSFETs [30]. This condition naturally causes our model calculations of carrier densities and characteristic times to deviate significantly from experiments. In particular, for transistors whose carrier movement has more than one dimension, such as those based on two-dimensional materials with one layer or multilayer. Therefore, we apply the α parameter to address the problem. If $\alpha = 1$, the device will closely approximate the one-dimensional transport condition. The F_j function is the complete Fermi-Dirac integral of order j. To accommodate transport containing many scattering events, it is convenient to write Eq. (5) as follows:

$$I_d = TWI_0\left(F_{1/2}(u) - F_{1/2}(u - u_d)\right), \tag{6}$$

where

$$T = \cos^2\left(\sqrt{\frac{\tau_t}{\alpha\tau_q}}\right)$$
$$\tau_t = \frac{2m_x L^2}{\hbar}\zeta$$
$$\tau_q = \frac{3\hbar}{2k_B T_e}\frac{F_{1/2}(u) - F_{1/2}(u - u_d)}{F_{3/2}(u) - F_{3/2}(u - u_d)}$$

after using the Taylor expansion of $\cos x = 1 - \frac{x^2}{2}$. By considering simple forms of conductivity, conductance, and mobility, i.e., $\sigma = nq\mu$, $G = \frac{\sigma A}{L}$, and $\mu = \frac{q\tau_t}{m_x}$, we demonstrate that τ_t represents the transport relaxation time. n and A are density and cross-sectional area, respectively. After assuming that $G \approx \frac{2q^2}{\hbar}$ and $n = \frac{1}{AL}$, and some algebraic rearrangement, $\tau_t \approx \frac{2m_x L^2}{\hbar}$, which is similar to τ_t in Eq. (6). Furthermore, when the MOSFET reaches saturation conditions, the Fermi-Dirac integral can be simplified with $F_{1/2}(u) \approx \frac{2}{3}u^{3/2}$ and $F_{3/2}(u) \approx \frac{4}{15}u^{5/2}$ for $\rho \gg 1$, then $\tau_q \approx \hbar/2\Gamma$ represents the quantum relaxation time, with $\Gamma = 8q\rho_0 Q_{inv}/15\hbar C_{eff} M_v$ defining the quantum level broadening. Eq. (6) states that the transmission depends on the relaxation time ratio, τ_t/τ_q, as a function of the voltages applied. In addition, when we apply a high voltage to our model, the quantum relaxation time can be greater than τ_c, the time required for the carrier to migrate from source to drain, leading to a non-physical meaning. To solve this problem, Eq. (6) should be valid under the following condition:

$$\lim_{(V_d,V_g)\to(\infty,\infty)} \tau_q - \tau_c = 0, \tag{7}$$

where $\tau_c = \frac{LQ_{inv}}{I_d}$. Eq. (7) implies that Δ, ζ, θ, and M_v depends on the V_g and V_d applied, such that it can be determined with a self-consistent iteration (SCI) procedure and fitting method. Furthermore, the transport and quantum relaxation times ratio in this study has another form, as follows:

$$\frac{\tau_t}{\tau_q} = \frac{L^2}{\lambda^2}, \tag{8}$$

where λ is the mean free path (MFP). In addition, Eq. (6) suggests that it is impracticable to fabricate ballistic

nanotransistors because the material must have zero effective mass to achieve maximum transmission. Thus, this condition may become the reason for modern transistor limits in nanoscale fabrication.

III. METHODOLOGY

To validate our work experimentally, we selected the monolayer MoS_2 FET from the work of Sebastian *et.al* [31]. The device has a bottom gate with Al_2O_3 as an oxide layer, with an effective oxide thickness (EOT) of 22 nm and a channel width of 5 μm. The gate electrode was made from a p^{++}-Si/TiN/Pt stack. Two monolayer MoS_2 FETs with channel lengths of 100 nm and 5 μm were analyzed. This study obtained the final parameters from non-linear least-squares fitting after the SCI procedure for M_v against the experimental data, I_d-V_d or I_d-V_g characteristics. Meanwhile, we solved Eq. (7) using the following numerical formula:

$$M_{v(new)} = M_{v(old)} + \omega \left(\frac{\tau_{q(lowest)} - \tau_c}{\tau_{q(lowest)}} \right) \tag{9}$$

where $\tau_{q(lowest)} - \tau_c$ is the smallest difference within an acceptable tolerance, and ω is a damping factor that can accelerate the convergence. The simulation accepted convergence when the dimensionless error $\left| \frac{\tau_{q(lowest)} - \tau_c}{\tau_{q(lowest)}} \right|$ was below the tolerance, and the R-squared was above the target tolerance. The SCI procedure steps are as follows: first select an initial guess for M_v, ζ, Δ, and θ. Then, implement a fitting process to update ζ, Δ, and θ. Next, use these updates to calculate the error and R-squared. If the error and R-squared do not reach the allowed tolerance, update M_v using Eq. (9) and reupdate for ζ, Δ, and θ with the fitting process. These steps are repeated until tolerance is reached.

The present study started with $\alpha = 1$ and increased incrementally in steps of 0.01, then performed SCI until convergence occurs. We take $I_{0t} = \frac{\sqrt{2}q(k_B T_e)^{3/2}}{\pi^2 \hbar^2} \sqrt{m_t}$ and $Q_0 = \frac{q k_B T_e m_d}{2\pi\hbar^2}$ as the variables for each device, where m_t and m_d represent the transverse and density of state (DOS) effective masses, respectively. Although these variables contain different quantum constant multipliers for different materials, they can compensate with M_v without changing the physical meaning of I_0 and ρ_0. We used $0.541m_0$ for all effective mass types of the monolayer MoS_2 device [50]. Here, m_0 is the rest mass of the electron. According to Sebastian *et.al*'s experiment [31], the threshold voltages of the devices have a median of 2.9 V and a mean of 2.8 V, with a standard deviation of 0.8 V, meaning they can vary by up to 3.6 V. Thus, in this study, the threshold voltage was set at 2.9 V in the Q_{inv} formula and the gate voltage domain at $V_g \geq 3.7$ V in the I_d-V_g characteristics to ensure our work is valid under strong inversion. The temperature was assumed to be 300 K. Further, this study set the oxide capacitance to 1.6×10^{-3} F/m^2 following the Sebastian *et.al* report. The error tolerance was accepted below 10^{-3} and an R-squared above 0.995.

IV. RESULTS AND DISCUSSION

Before discussing the dominant scattering mechanism in two-dimensional MoS_2 FETs, the drain current model accuracy in Eq. (6) was validated against the device data from Sebastian *et.al*. The validation included current characteristics, velocity saturation, field-effect mobility, DIBL, and body factors to show the advantages and limitations of our model. Figures 1(a) and (b) represent the SCI procedure results for the I_d-V_d characteristics of devices with 100-nm and 5-μm channel lengths. In Fig. 1(a), the model prediction for a 100-nm channel length had an R-squared from 0.9995 to 0.9998 for each gate voltage, except for 12 V, which gave around 0.9992. Furthermore, Fig. 1(b) shows that the model accuracy for a 5-μm channel length increased from 0.99998 to 0.9999, only at a gate voltage of 4 V gave around 0.9976. The data from a device with a 100-nm channel length exhibited NDR current characteristics. When the gate voltage is high, the behavior becomes more evident as the gate voltage increases. However, the 5-μm channel length did not show this behavior. The R-squared results confirmed that this model is capable of capturing NDR behavior. In addition, we benchmarked our present model against another ballistic limit model built without considering the paradigm solution between WKB approximation and small scattering for adequacy reasons [32]. This benchmark model is summarized in Supplementary Note 1. Supplementary Figure 1 indicates that it fails to capture the NDR phenomenon of the I_d-V_d characteristics for a channel length of 100 nm, consistent with a first-principles study for a two-dimensional MoS_2 transistor [14]. For the 5-μm channel length, the benchmark model demonstrates improved outcomes but remains less accurate than our model. Thus, the paradigm overlap between the WKB approximation and small scattering has a meaningful solution for the ballistic series model applied to the devices. A damping parameter equal to one was used for all SCI procedures. This damping can speed up SCI procedures without significantly affecting M_v. To demonstrate this statement, we performed 100-nm channel length SCI procedures for I_d-V_d characteristics at a 6 V gate voltage with different dampings to plot M_v and the progressive error, as presented in Fig. 1(c). In the figure, increasing the damping decreases the number of SCI iterations while maintaining M_v. However, although this damping allowed the procedure to accelerate, it also increased the error rate and may have triggered divergence conditions. Therefore, some experiments with initial values under bulk and small scale transistor physics intuitions are needed to test these conditions. In addition, lower and upper bound predictions of the non-linear least-square fitting during SCI are also required to ensure safe initial parameters for use in this model. Meanwhile, Fig. 1(d) depicts the parameters for each gate voltage extracted from the SCI procedure for the I_d-V_d characteristics. Here, the alpha parameter for 100-nm and 5-μm channel lengths is 2.8 and 43.3, respectively.

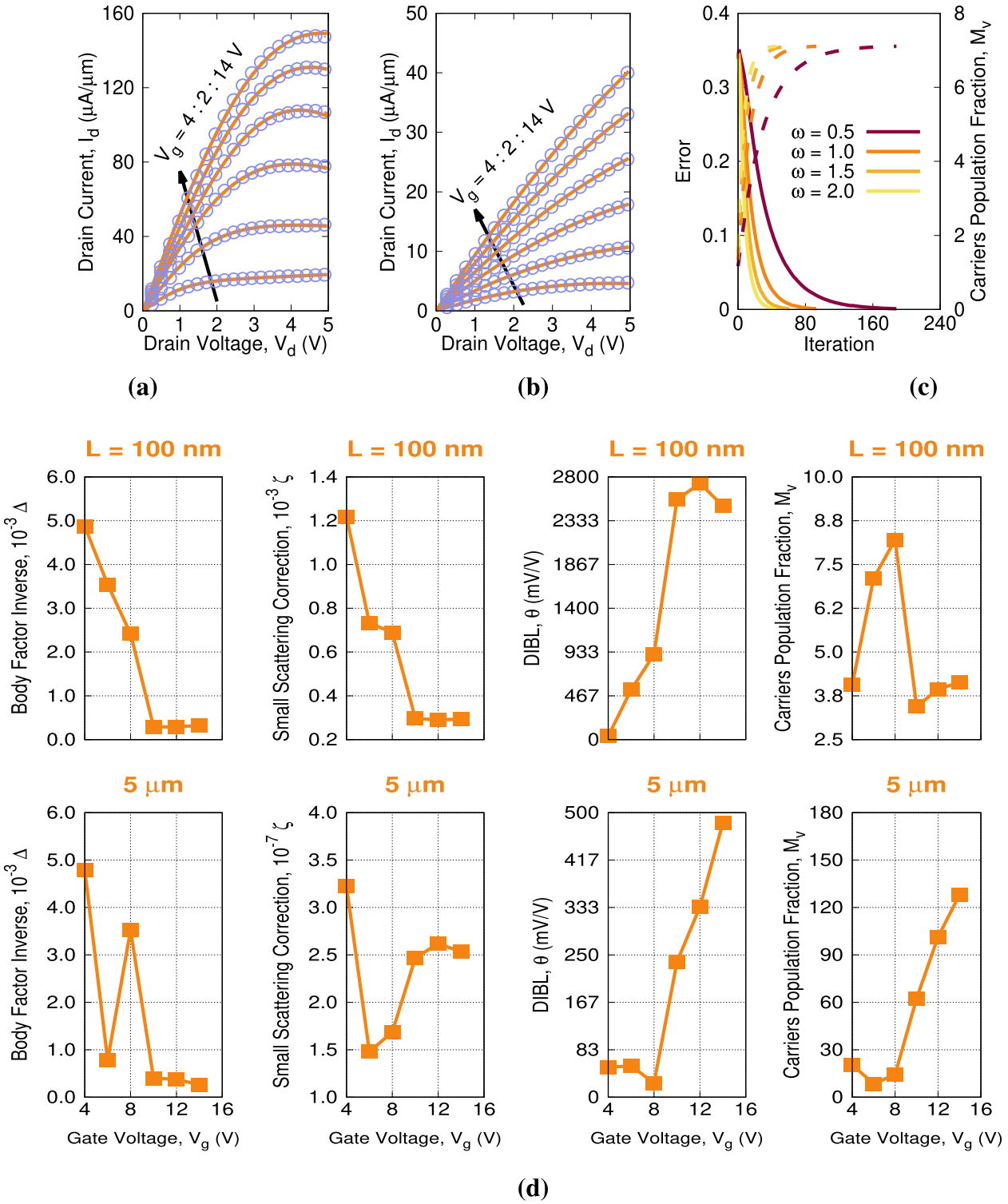

FIGURE 1. Validation results for monolayer MoS_2 FET I_d-V_d characteristics with (a) 100-nm and (b) 5-μm channel lengths. The solid line and open circle represent the model result and experiment data, respectively. (c) Damping variation effect on 10-nm channel length SCI procedures for I_d-V_d characteristics at 6 V gate voltage. The solid and dashed lines represent the dimensionless error and M_v, respectively. (d) Model parameters for each gate voltage extracted from the SCI procedure for the I_d-V_d characteristic of 100-nm and 5-μm channel lengths.

The alpha of this device indicates that the characteristic current originates from non-one-dimensional carrier transport.

Further, the parameters in Fig. 1(d) were used to calculate the carrier velocity using the formula $v = I_d/Q_{inv}$ and compared to statistical measures from the experimental work.

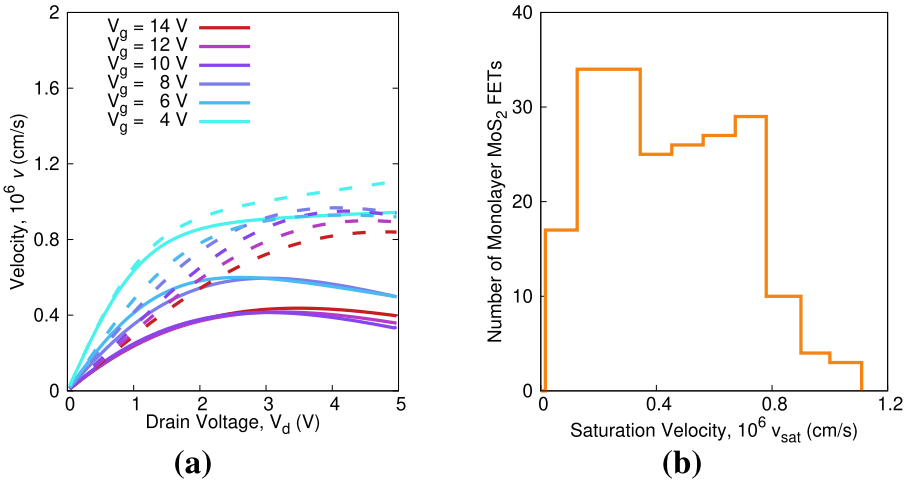

FIGURE 2. (a) Velocity calculation from the present model for a 100-nm channel. The solid and dashed lines represent the calculation with and without the DIBL phenomenon, respectively. (b) The statistical population of saturation velocities from the experiment [31].

For an adequate comparison, two velocity calculations were performed with and without the DIBL of charge inversion. This was done because the experiment ignored the DIBL while collecting the saturation velocity, v_{sat}. Figure 2(a) shows the velocities for the 100-nm channel. The figure implies that the saturation velocity calculations of 0.75×10^6 to 0.95×10^6 cm/s are close to the best results in the experiment. When considering the DIBL phenomenon, the calculated saturation velocity was about 0.3×10^6 to 0.6×10^6 cm/s, which is in the most populous range according to the experimental data, as confirmed in Fig. 2(b).

Furthermore, we show our model validation for the I_d-V_g characteristics, field-effect mobility, and statistical body factors extracted from the experimental data. Figures 3(a) and (b) demonstrate the I_d-V_g and transfer characteristics. From the figures, the model accuracy for a 100-nm channel is generally stable at around 0.9999 R-squared value, especially at a lower drain voltage. However, the accuracy decreased exponentially from 0.9981 to 0.9957 with increasing drain voltage for a 5-μm channel. This decrease in accuracy probably arises from the strong inversion assumption used in this model. This assumption prevents this model from accounting for small currents flowing in a weak inversion zone. Figure 3(c) displays the parameters for each drain voltage extracted from the SCI procedure for I_d-V_g characteristics. The same α values were used as for the I_d-V_d characteristic SCI procedure.

Strong inversion also emphasized errors when the field-effect mobility and body factor were analyzed. Here, the formula $\mu_{gm} = (L/WC_{ox}V_d)\left(dI_d/dV_g\right)$ was used to calculate the mobility with parameters taken from Fig. 3(c). Figures 4(a) and (b) show the mobility results for 100-nm and 5-μm channel monolayer MoS_2 FETs, respectively. Generally, this model follows the experimental data trend in the strong inversion zone for each drain voltage. It is close to the mobility curve peak in the case of a short channel, especially at low drain voltages, but the prediction deviates significantly from the experimental data if used for the long-channel devices. When considering the 100-nm channel, Fig. 3(c) shows exponential growth in Δ. Based on the model predictions, the body factor decreased exponentially for each increase in drain voltage from 806.6 to 112.6. However, this model predicts 416.4 on average, which is 4.1% away from the maximum experimental results, as shown in Fig. 4(c). In contrast to these results, this model predicted a body factor beyond the experimental data for a 5-μm channel. The average prediction was 174 times the maximum statistical value. These results provide information on the limited accuracy of this work: the field-effect mobility and body factor for the long channel cannot be calculated accurately with this model under the strong inversion assumption.

Next, the prediction of the dominant scattering mechanisms of two-dimensional monolayer MoS_2 FETs with our model is discussed. For this purpose, the model parameters in Fig. 1 were used to calculate the single-particle and transport relaxation times ratio, MFP, and transmission. These parameters were used to explore the carrier scattering mechanism interpreted from the I_d-V_d characteristic data. Further, these calculations are presented against ρ_0 to identify the dominant scattering. Figure 5 shows the results for 100-nm and 5-μm channel lengths.

Figure 5(a) shows that the 100-nm channel length monolayer MoS_2 FET has a low relaxation time ratio, which indicates that short-range scattering controls carrier transport [33]. The figure shows that the charge carrier density dependence decreases when the relaxation time ratio is high, suggesting that the carriers undergo small-angle scattering relative to the incident direction, which is anisotropic in character. When the ratio decreases and the density grows, the dependence strengthens, indicating an increase in the angle associated with isotropic scattering. Thus, scattering

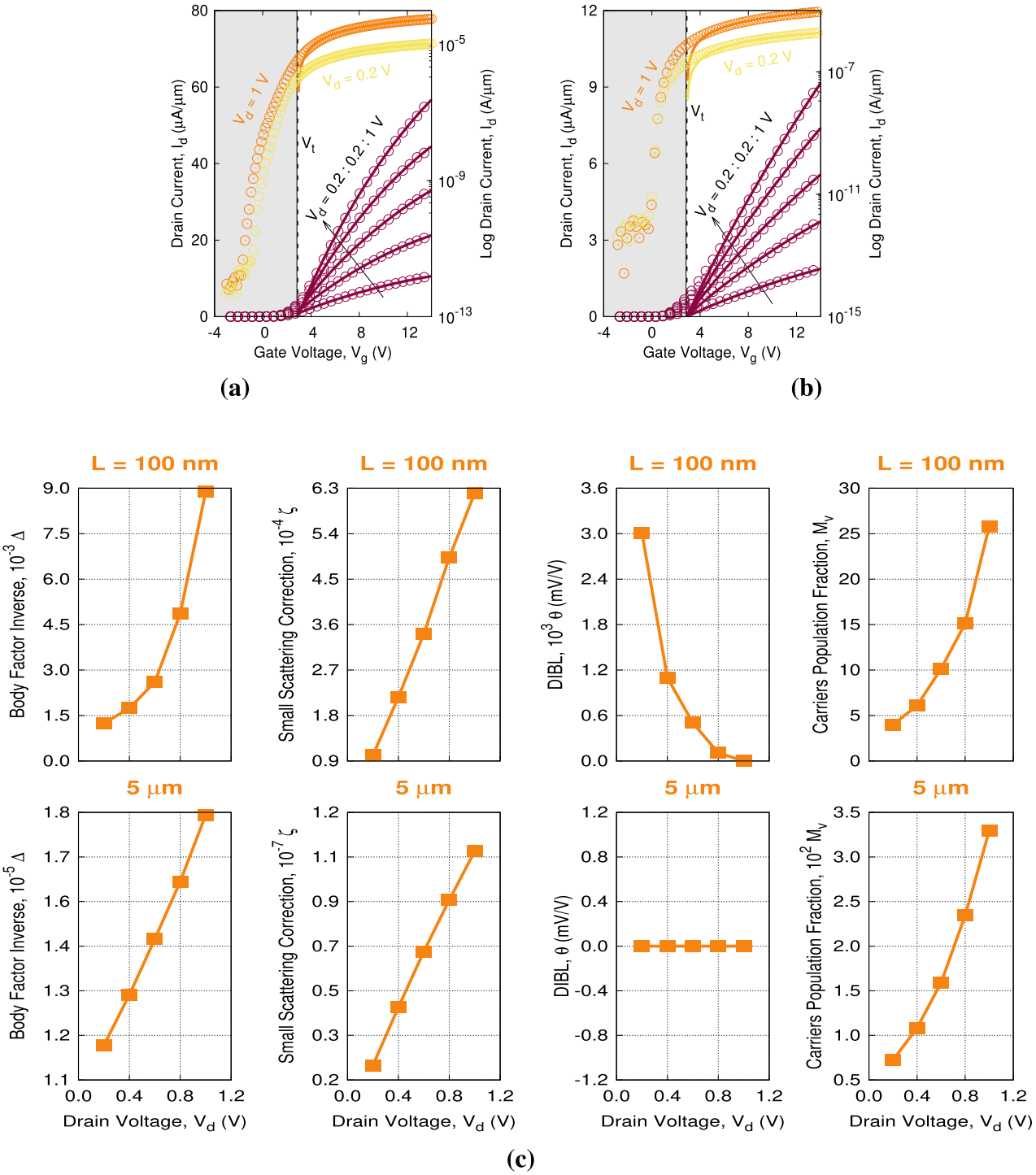

FIGURE 3. Validation results for monolayer MoS_2 FET I_d-V_g characteristics with (a) 100-nm and (b) 5-μm channel lengths. The open circles and solid lines represent experimental data and the present model, respectively. The orange and yellow colors represent the transfer of the I_d-V_g characteristics into the log scale. The gray background represents a weak inversion zone. (c) Model parameters for each drain voltage extracted from the SCI procedure of the I_d-V_g characteristics for the 100-nm and 5-μm channel lengths.

within the device experiences a mechanism transition from anisotropy to isotropy as the gate voltage increases. It seems surface roughness controlled the mechanism at low gate and drain voltages, while impurities dominated at high voltages. This mechanism differs from silicon-based nanoscale FETs, in which the surface roughness effect becomes more significant at high voltages [34]. The difference in surface roughness character may result from the polycrystalline Pt in the gate electrode stack of monolayer MoS_2 FETs. Sebastian et. al. reported that Pt usage reduced hysteresis

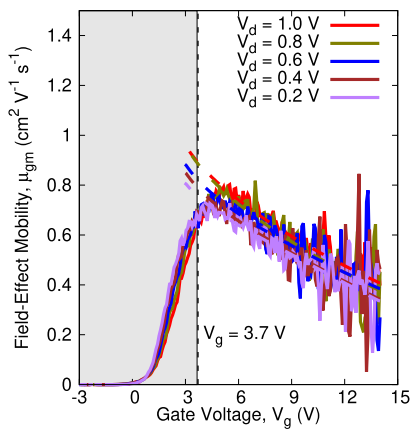

(a)

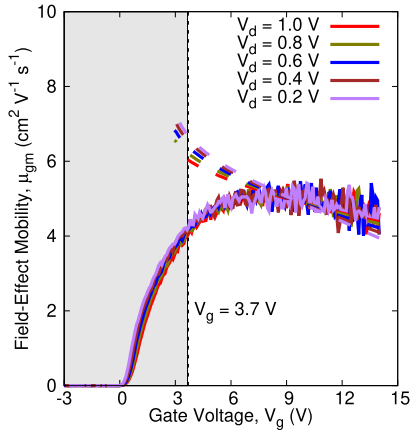

(b)

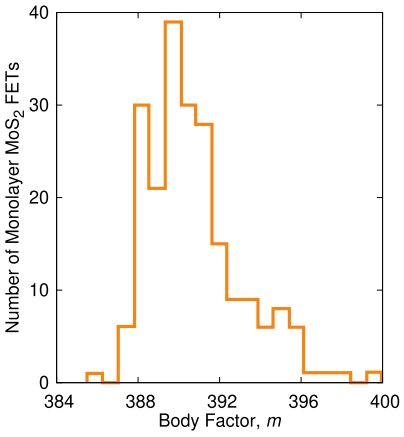

(c)

FIGURE 4. Validation results for monolayer MoS_2 FET field-effect mobility for (a) 100-nm and (b) 5-μm channel lengths. The solid and dashed lines represent the experimental results and the present model, respectively. The gray background represents the area beyond the gate voltage domain in the I_d-V_g characteristic SCI procedure. (c) The body factor statistics were extracted from the experimental data [31].

and trap state effects [31]. The polycrystalline Pt introduces little surface roughness to the final Al_2O_3 surface, with a root mean square roughness of 0.7 nm. As a result, surface roughness is insignificant at high voltages for monolayer MoS_2 FET. The surface roughness produced a barrier potential for carriers at the four lowest subband energies, leading to tunnel scattering. Only carriers with three narrow band energies remained trapped while the others continued toward the drain to produce an NDR phenomenon at high voltages, according to a first-principle study [14]. Due to the two-dimensional structure of the device, the impurities encouraged carrier transport to undergo a thermionic emission mechanism [35]. This interpretation is explained because tunnel scattering is inherently more anisotropic than thermionic emission. The figure reveals that only a few carrier densities contribute to tunnel scattering due to the surface roughness of the small device. Because this model was developed based on a single subband, the carrier density calculations yielded small predictions for anisotropy, especially at low gate voltages. Therefore, the model in this work requires further development for a better interpretation. Other simulation studies have reported that surface roughness and impurities can significantly influence drain current device performance [36], [37]. However, the model in the current work showed a shift in the scattering mechanism from surface roughness to impurities with increasing gate voltage, providing a physical insight beyond those studies and experimental results. In addition, the MFP length expanded until it reached a maximum of no more than 60 nm due to the isotropic state at high gate voltages. As a result, carrier transmission in this device also appeared to stop rising at 0.3 for high gate voltages, as shown in Fig. 5(b).

Meanwhile, Fig. 5(c) shows the relaxation time ratio results for the monolayer MoS_2 FET with a 5-μm channel length. The ratio is large, indicating that long-range scattering controls carrier transport. Coulomb scattering through the interface-trapped electron mechanism becomes more possible than when impurities are present. The body factor exceeded the one calculated from our model, and the experimental data confirmed that interface traps were present between the monolayer and the dielectric. Structural defects, such as sulfur vacancies, photoresist residue from lithography, and the wet transfer process likely caused this interface. These calculations indicate that long-range scattering on the device caused many collisions on the carrier, reducing the MFP length to less than half of the channel length. This situation affected low carrier transmission below 0.04, as shown in Fig. 5(d). The carrier density of the device was approximately 0.075 lower than that of a 100-nm channel device. This low density contributed to the small drain current produced by the device.

Generally, the monolayer MoS_2 FETs with both channel lengths had a carrier density-dependent relaxation time ratio. This dependence indicates that the drain current produced in these devices depends on mobility and does not originate from ballistic transport. In addition, the experimental data did not display the phonon effect in monolayer MoS_2 FETs, whereas Monte Carlo and first principles simulations have

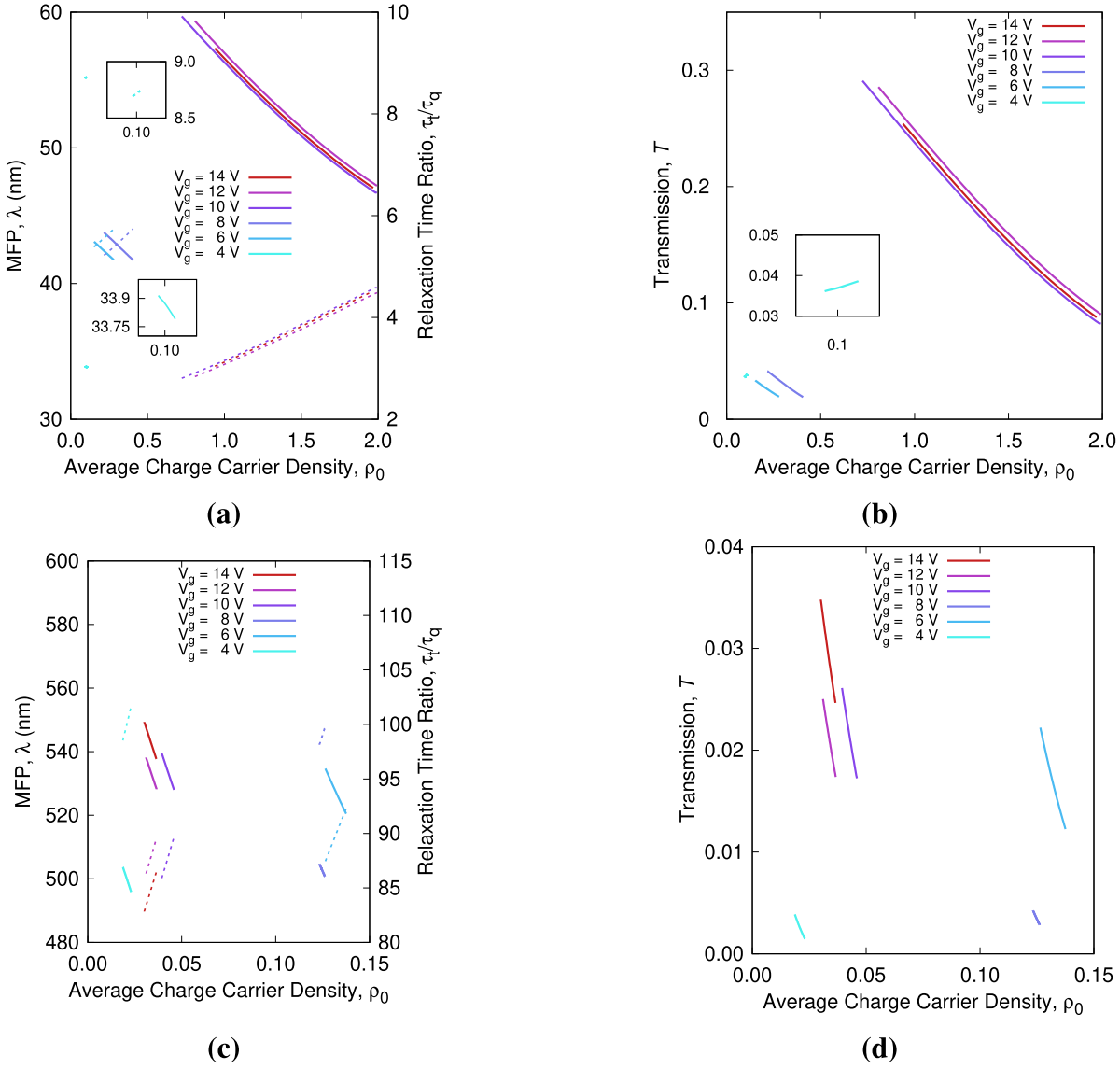

FIGURE 5. The MFP, τ_t/τ_q ratio, and transmission calculation results as a function of ρ_0. (a), (b) and (c), (d) are for 100-nm and 5-μm channel lengths, respectively. The solid and dashed lines in (a) and (c) represent the calculations for MFP and τ_t/τ_q, respectively.

shown that scattering due to phonons also affects carrier transport [5], [14], [36], [38], [39], [40]. However, the current model developed in this study did not account for phonon effects on the relaxation time ratio due to the simple form of the potential $U(\varepsilon\xi)$.

V. CONCLUSION

This work developed a comprehensive analytical model for two-dimensional MoS_2 FET with embedded single-particle and transport relaxation times. The relaxation time ratio was used to investigate the dominant scattering mechanism of carrier transport. The model has five parameters that depend on the applied gate and drain voltages obtained through the SCI procedure and fitting process. Experimental data from monolayer MoS_2 FETs was used to support our model. As a result, our model accurately captures the NDR phenomenon and interface traps of the device, which cannot be explained with the conventional ballistic model. There was a shift in the short-range scattering mechanism from anisotropy toward isotropy for the short-channel length device as the gate voltage increased. The anisotropy and isotropy mechanisms are mediated by tunnel scattering and thermionic emission, respectively, in agreement with DFT and Monte Carlo simulation studies. In contrast, long-range scattering through the interface trap electrons limited carrier transport in long-channel devices. Thus, our model can reveal the dominant scattering mechanisms that restrict the performance of two-dimensional MoS_2 FETs primarily due to the NDR phenomenon and interface traps directly from the current-voltage characteristics curve, reducing the need for complex measurements and simulations.

ACKNOWLEDGMENT

The authors would like to thank Prof. Saptarshi Das and Amritanand Sebastian for providing the experimental data to support this work. We would also like to thank Dr. Muhammad Rizqie Arbie, Dr. Dhewa Edikresnha, and Prof. Rachmat Hidayat for the fruitful discussions.

REFERENCES

[1] S. Das Sarma and F. Stern, "Single-particle relaxation time versus scattering time in an impure electron gas," *Phys. Rev. B*, vol. 32, no. 12, pp. 8442–8444, Dec. 1985.
[2] E. H. Hwang and S. Das Sarma, "Single-particle relaxation time versus transport scattering time in a two-dimensional graphene layer," *Phys. Rev. B*, vol. 77, no. 19, May 2008, Art. no. 195412.
[3] B. Sadhukhan, R. Chimata, B. Sanyal, and A. Mookerjee, "Magnetization dynamics in Fe_xCo_{1-x} in presence of chemical disorder," *Magnetochemistry*, vol. 9, no. 2, p. 44, Jan. 2023.
[4] S. Streib, N. Vidal-Silva, K. Shen, and G. E. W. Bauer, "Magnon-phonon interactions in magnetic insulators," *Phys. Rev. B*, vol. 99, no. 18, May 2019, Art. no. 184442.
[5] T. Gunst, T. Markussen, K. Stokbro, and M. Brandbyge, "First-principles method for electron-phonon coupling and electron mobility: Applications to two-dimensional materials," *Phys. Rev. B*, vol. 93, no. 3, Jan. 2016, Art. no. 035414.
[6] T. Sohier, M. Calandra, C.-H. Park, N. Bonini, N. Marzari, and F. Mauri, "Phonon-limited resistivity of graphene by first-principles calculations: Electron-phonon interactions, strain-induced gauge field, and Boltzmann equation," *Phys. Rev. B*, vol. 90, no. 12, Sep. 2014, Art. no. 125414.
[7] P. P. Poduval, K. Laubscher, and S. Das Sarma, "Apparent Kondo effect in Moiré transition metal dichalcogenide bilayers: Heavy fermions versus disorder," *Phys. Rev. B*, vol. 108, no. 8, Aug. 2023, Art. no. 174204.
[8] Y.-T. Tu and S. Das Sarma, "Wiedemann-franz law in graphene in the presence of a weak magnetic field," *Phys. Rev. B*, vol. 108, no. 24, Dec. 2023, Art. no. 085401.
[9] S. Sykora, J. Schoop, L. Graf, G. Shipunov, I. V. Morozov, S. Aswartham, B. Büchner, C. Hess, R. Giraud, and J. Dufouleur, "Disorder-induced coupling of weyl nodes in WTe2," *Phys. Rev. Res.*, vol. 2, no. 3, Jul. 2020, Art. no. 033041.
[10] J.-H. Hur, J. Park, D.-K. Kim, and S. Jeon, "Model for the operation of a monolayer MoS_2 thin-film transistor with charges trapped near the channel interface," *Phys. Rev. Appl.*, vol. 7, no. 4, Apr. 2017, Art. no. 044030.
[11] A. V. Bruce, S. Liu, J. N. Fry, and H.-P. Cheng, "Clar's goblet on graphene: Field-modulated charge transfer in a hydrocarbon heterostructure," *Phys. Rev. B, Condens. Matter*, vol. 102, Sep. 2020, Art. no. 115415.
[12] J. Chang, L. F. Register, and S. K. Banerjee, "Topological insulator Bi_2Se_3 thin films as an alternative channel material in MOSFETs," *J. Appl. Phys.*, vol. 115, no. 8, 2014, Art. no. 084506.
[13] J. Chang, L. F. Register, and S. K. Banerjee, "Topological insulator Bi_2Se_3 thin films as an alternative channel material in MOSFETs," *J. Appl. Phys.*, vol. 112, no. 12, 2012, Art. no. 124511.
[14] Á. Szabó, R. Rhyner, and M. Luisier, "Ab initio simulation of single- and few-layerMoS_2 transistors: Effect of electron-phonon scattering," *Phys. Rev. B*, vol. 92, no. 3, Jul. 2015, Art. no. 035435.
[15] F. A. Noor, I. Syuhada, T. Winata, F. Yu, M. F. Fatahilah, H. S. Wasisto, and K. Khairurrijal, "Investigation of electrical behaviors observed in vertical GaN nanowire transistors using extended Landauer-Büttiker formula," *IEEE Access*, vol. 9, pp. 2913–2923, 2021.
[16] V. R. Murnal and C. Vijaya, "A quasi-ballistic drain current, charge and capacitance model with positional carrier scattering dependency valid for symmetric DG MOSFETs in nanoscale regime," *Nano Converg.*, vol. 6, no. 1, pp. 1–24, Jun. 2019.
[17] S. Rakheja, M. S. Lundstrom, and D. A. Antoniadis, "An improved virtual-source-based transport model for quasi-ballistic transistors—Part I: Capturing effects of carrier degeneracy, drain-bias dependence of gate capacitance, and nonlinear channel-access resistance," *IEEE Trans. Electron Devices*, vol. 62, no. 9, pp. 2786–2793, Sep. 2015.
[18] M. Lundstrom and Z. Ren, "Essential physics of carrier transport in nanoscale MOSFETs," *IEEE Trans. Electron Devices*, vol. 49, no. 1, pp. 133–141, Aug. 2002.
[19] J. Lee, "Unified model of shot noise in the tunneling current in sub-10 nm MOSFETs," *Nanomaterials*, vol. 11, no. 10, Oct. 2021, Art. no. 2759.
[20] Z. Yan, G. Gou, J. Ren, F. Wu, Y. Shen, H. Tian, Y. Yang, and T.-L. Ren, "Ambipolar transport compact models for two-dimensional materials based field-effect transistors," *Tsinghua Sci. Technol.*, vol. 26, no. 5, pp. 574–591, Oct. 2021.
[21] A. V. Lebedev and V. M. Vinokur, "Heat generation due to the Anderson catastrophe in mesoscopic devices," *Phys. Rev. B*, vol. 102, no. 19, Nov. 2020, Art. no. 195111.
[22] N. Haratipour, S. Namgung, S.-H. Oh, and S. J. Koester, "Fundamental limits on the subthreshold slope in Schottky source/drain black phosphorus field-effect transistors," *ACS Nano*, vol. 10, no. 3, pp. 3791–3800, Mar. 2016.
[23] L. D. Landau and E. M. Lifshitz, *Quantum Mechanics Non-relativistic Theory*, 2nd ed. New York, NY, USA: Pergamon, 1956.
[24] M. V. Berry and K. E. Mount, "Semiclassical approximations in wave mechanics," *Rep. Prog. Phys.*, vol. 35, no. 1, pp. 315–397, Jan. 1972.
[25] H. Li, J. Liang, Q. Wang, F. Liu, G. Zhou, T. Qing, S. Zhang, and J. Lu, "Device performance limit of monolayer $SnSe_2$ MOSFET," *Nano Res.*, vol. 15, no. 3, pp. 2522–2530, Mar. 2022.
[26] A. K. Chatterjee, M. Kushwaha, and B. Prasad, "Analytical model for drain current of a ballistic MOSFET," *Silicon*, vol. 13, no. 6, pp. 1777–1785, Jun. 2021.
[27] S. Guo, Y. Wang, X. Hu, S. Zhang, H. Qu, W. Zhou, Z. Wu, X. Liu, and H. Zeng, "Ultrascaled double-gate monolayer MOSFETs for high-performance and low-power applications," *Phys. Rev. Appl.*, vol. 14, Oct. 2020, Art. no. 044031.
[28] K. Natori, "Ballistic metal-oxide-semiconductor field effect transistor," *J. Appl. Phys.*, vol. 76, no. 8, pp. 4879–4890, Oct. 1994.
[29] K. Y. Bliokh, V. D. Freilikher, and N. M. Makarov, "Scattering by one-dimensional smooth potentials: Between WKB and born approximation," *Phys. E, Low-Dimensional Syst. Nanostruct.*, vol. 27, nos. 1–2, pp. 262–269, Mar. 2005.
[30] M. Wolf, *The Physics of Computing*. San Mateo, CA, USA: Morgan Kaufmann, 2017, pp. 13–62.
[31] A. Sebastian, R. Pendurthi, T. H. Choudhury, J. M. Redwing, and S. Das, "Benchmarking monolayer MoS_2 and WS_2 field-effect transistors," *Nature Commun.*, vol. 12, no. 1, p. 693, Jan. 2021.
[32] J. U. Lee, R. Cuduvally, P. Dhakras, P. Nguyen, and H. L. Hughes, "Two-parameter quasi-ballistic transport model for nanoscale transistors," *Sci. Rep.*, vol. 9, no. 1, p. 525, Jan. 2019.
[33] A. Gold, "Scattering time and single-particle relaxation time in a disordered," *Phys. Rev. B, Condens. Matter*, vol. 38, pp. 10798–10811, Nov. 1988.
[34] A. Cresti, M. G. Pala, S. Poli, M. Mouis, and G. Ghibaudo, "A comparative study of surface-roughness-induced variability in silicon nanowire and double-gate FETs," *IEEE Trans. Electron Devices*, vol. 58, no. 8, pp. 2274–2281, Aug. 2011.
[35] P. Wang, S. Han, and R. Quhe, "Quantum transport simulation of the two-dimensional GaSb transistors," *J. Semiconductors*, vol. 42, no. 12, Dec. 2021, Art. no. 122001.
[36] H. Tanaka and N. Mori, "Modeling of carrier scattering in MOS inversion layers with large density of interface states and simulation of electron Hall mobility in 4H-SiC MOSFETs," *Jpn. J. Appl. Phys.*, vol. 59, no. 3, Mar. 2020, Art. no. 031006.
[37] X. Ma, Y. Gong, J. Wu, Y. Li, and J. Chen, "Impacts of atomistic surface roughness on electronic transport in n-type and p-type MoS_2 field-effect transistors," *Jpn. J. Appl. Phys.*, vol. 58, no. 11, Oct. 2019, Art. no. 110905.
[38] A. Afzalian, "Ab initio perspective of ultra-scaled CMOS from 2D-material fundamentals to dynamically doped transistors," *npj 2D Mater. Appl.*, vol. 5, no. 1, Jan. 2021, Art. no. 5691.
[39] Z. Yu, Z.-Y. Ong, S. Li, J.-B. Xu, G. Zhang, Y.-W. Zhang, Y. Shi, and X. Wang, "Analyzing the carrier mobility in transition-metal dichalcogenide MoS_2 field-effect transistors," *Adv. Funct. Mater.*, vol. 27, no. 19, 2017, Art. no. 1604093.
[40] Y. Cai, G. Zhang, and Y.-W. Zhang, "Polarity-reversed robust carrier mobility in monolayer MoS_2 nanoribbons," *J. Amer. Chem. Soc.*, vol. 136, no. 17, pp. 6269–6275, Apr. 2014.

FATIMAH AROFIATI NOOR (Member, IEEE) received the Ph.D. degree in physics from the Institut Teknologi Bandung (ITB), in 2010. In 2010, she joined the Faculty of Mathematics and Natural Sciences, ITB, as a member, where she is currently a Professor. Since 2021, she has been the Head of Undergraduate Program in Physics at ITB. Her current research interest includes simulation on electronics.

IBNU SYUHADA received the Dr. degree in physics from the Institut Teknologi Bandung (ITB), in 2020. He is a Researcher at the Cahaya Putra Ilmu Foundation. His research interest includes semiconductors for nanoelectronics.

TOTO WINATA received the Ph.D. degree in atomic physics from Murdoch University, Australia, in 1991. Since 2008, he has been a Professor with the Faculty of Mathematics and Natural Sciences, Institut Teknologi Bandung. From 2016 to 2018, he was the Head of the Physics of Electronic Materials Research Division. His research interest includes semiconductors for optoelectronics.

KHAIRURRIJAL KHAIRURRIJAL (Member, IEEE) received the Dr.Eng. degree in electrical engineering from the Graduate School of Engineering, Hiroshima University, Japan, in 2000. Since 2010, he has been a Professor with the Faculty of Mathematics and Natural Sciences, Institut Teknologi Bandung. Since 2019, he has been the Head of the Physics of Electronic Materials Research Division, with activities in the fields of semiconductors for optoelectronics, nanosensors, and nanoelectronics. He received the National Outstanding Lecturer Award from the Ministry of National Education of Republic of Indonesia (RI), in 2011; the Habibie Award in the field of Basic Science from the Foundation for Human Resources in Science and Technology-The Habibie Center, in 2017; and the Academic Leader Award in the field of basic science from the Ministry of Research and Higher Education of RI, in 2019.